Paper I

I

Second-harmonic reflectors on 128° $LiNbO_3$

S. Lehtonen, V. P. Plessky,
J. Koskela, and M. M. Salomaa

S. Lehtonen, V. P. Plessky, J. Koskela, and M. M. Salomaa, "Second harmonic reflectors on 128° $LiNbO_3$", IEEE Transactions on Ultrasonics, Ferroelectrics, and Frequency Control, Vol. 50, No. 8, August 2003, pp. 972-978.

Second-Harmonic Reflectors on 128° $LiNbO_3$

Saku Lehtonen, Victor P. Plessky, *Senior Member, IEEE*, Julius Koskela, *Member, IEEE*, and Martti M. Salomaa, *Member, IEEE*

***Abstract*—In this work, we study theoretically the operation of long surface acoustic wave reflectors, comprising a large number of electrodes, at the fundamental and second harmonic frequencies on the 128° $LiNbO_3$ substrate for various electrode thicknesses and metallization ratios. Numerical simulations utilizing tailored test structures and time gating indicate that the reflectivity of the second-harmonic reflectors can be very high for certain geometries. Furthermore, our simulations suggest that inside the stopband the total losses for the second harmonic are of the same order as those for operation at the fundamental harmonic.**

I. Introduction

The classic 128° YX-$LiNbO_3$ crystal cut is widely used in TV surface acoustic wave (SAW) filters and, recently, in SAW tags, because of its low level of spurious bulk-wave generation and the relatively high piezoelectric coupling. However, the factor limiting the range of applications of 128° $LiNbO_3$ is the weak reflectivity of the aluminium electrodes at the fundamental harmonic frequency. Low reflectivity implies a large number of fingers in the reflector gratings, which complicates the efforts to comply with the size limitations. Moreover, for certain applications, such as low-loss devices or SAW tags, a low reflectivity is quite a restrictive feature.

The motivation for studying higher-harmonic reflectors is that considerable reflectivities may be obtained on substrates, such as 128° YX-$LiNbO_3$, where the reflectivity at the fundamental harmonic is low [1]. This result is to some extent unexpected since the conventional model of reflections is that of a mismatched delay line, see, e.g., [2], which yields for the reflectivity κ of a single electrode a sinusoidal dependence on the width of the electrode a, $\kappa \propto \sin(\beta a)$ with $\beta = 2\pi/\lambda$. The typical reasoning is that this function attains a maximum for an electrode having the width of a quarter of the wavelength λ. Evidently, the same function yields zero reflectivity for an electrode half a wavelength wide. At least for strong reflectors, none of the statements is actually valid, since the contribution of the energy-storage effect [1] is known to result in a finite reflectivity for half-wavelength electrodes. Moreover, even without mass-loading, the purely electrical contribution to the reflectivity for a $\lambda/2$-wide electrode is quite high [3]. This strong reflectivity of the second-harmonic reflectors is an intriguing observation. A combination of the low spurious level of 128° YX-$LiNbO_3$ with a high reflectivity would be very attractive for SAW sensor and tag applications.

The properties of reflectors with finite electrode thickness at harmonic frequencies have not been extensively studied. Experimental work in this direction has been carried out, e.g., by Campbell and Edmonson [4], who studied the properties of a harmonic one-port resonator on 64° YX-cut $LiNbO_3$.

In this work, we attempt to characterize, by theoretical means, long reflectors comprising a large number of electrodes. As our method of investigation, we apply a two-step procedure. First, the velocities v and the reflectivities in the gratings are initially characterized using a simulator applying the finite element and boundary element methods (FEM, BEM) for infinite periodic electrode arrays [5]. Considerably slower, but more realistic, FEM/BEM simulations of finite structures [6] are then applied to evaluate the reflectivity and the attenuation. Preliminary results of this work have been published in [7] and [8].

II. Simulations of Infinite Periodic Arrays

The infinite periodic simulator was used to extract the velocity v and normalized reflectivity $\kappa\lambda_0$ in a second-harmonic grating as a function of electrode thickness h/λ_0 and metallization ratio a/λ_0. To evaluate the accuracy of the infinite periodic approximation, the coupling-of-modes model (COM) was employed to characterize a test structure encompassing an interdigital transducer, IDT (v and $\kappa\lambda_0$ for fundamental-mode operation), and two reflectors operating at the second harmonic frequency (v and $\kappa\lambda_0$ for second-harmonic operation; see Fig. 1(a)).

There are methodological difficulties related to the numerical characterization of infinite periodic electrode arrays operating at the second harmonic. For even-order harmonic frequencies $f_{2n} = nv/p$, where p denotes the pitch of the array, the electromechanical coupling coefficient of the SAW eigenmodes tends to vanish. In this case the electrodes are separated by a distance equal to an integer number of λ and, for synchronous excitation, the waves generated by adjacent fingers in a standard IDT are in opposite phase and interfere destructively. To circumvent the problems with electric sources, we follow the general idea of

Manuscript received April 15, 2002; accepted March 20, 2003. This work was supported by Thales Microsonics SA. The first author (SL) also acknowledges the Academy of Finland for support within the Graduate School in Technical Physics and the NOKIA Foundation for a scholarship.

S. Lehtonen, J. Koskela, and M. M. Salomaa are with the Materials Physics Laboratory, P.O. Box 2200, FIN–02015 HUT, Finland (e-mail: saku@focus.hut.fi).

V. P. Plessky is with Thales Microsonics, SAW Design Bureau, Fahys 9, CH–2000 Neuchâtel, Switzerland.

J. Koskela's present address is Nokia Research Center, P.O. Box 407, FIN–00045 Nokia Group, Finland.

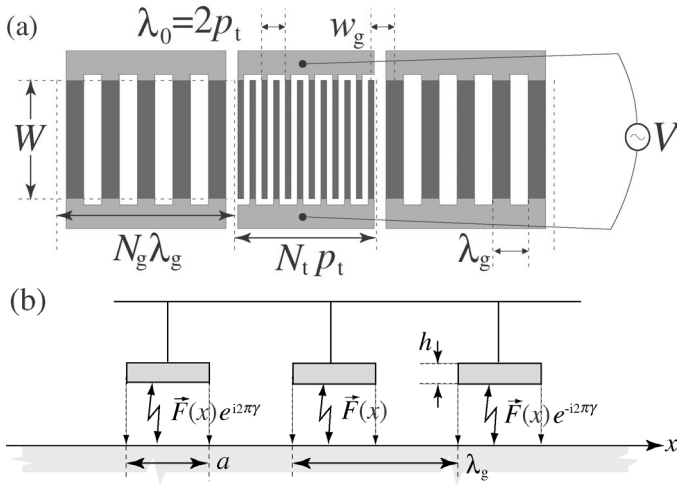

Fig. 1. (a) Resonator with second-harmonic reflectors. p_t is the pitch in the transducer, λ_g is the period in the reflector grating. (b) Numerical experiment, where an infinite periodic grating is driven by mechanical forces acting at the interface between the electrodes and the substrate.

mechanical excitation, a possibility mentioned by Ventura *et al.*, in the context of fundamental harmonic operation [9]. Mechanical sources, i.e., oscillating stress forces $\vec{T}(x)$ acting at the electrode-substrate interface, are employed to drive the grating in the harmonic configuration with the excitation wavenumber γ close to zero (see Fig. 1(b)). The resulting resonances in such a numerical experiment enable one to detect the edges of the stopband and, hence, the center frequency and reflectivity.

III. Test Structure for Rigorous Simulations

The complete dispersion relation—especially the attenuation due to the scattering into bulk waves—remains difficult to evaluate from simulations of infinite electrode arrays. Further complications are the potentially significant losses due to SAW-BAW scattering at the discontinuities between the reflectors and the IDT, not included in the simulations for periodic arrays. Hence, rigorous FEM/BEM simulations of finite structures [6] are carried out. The COM model is employed to analyze the results of the simulations and to compare them with those of the periodic FEM/BEM simulator.

By introducing proper test structures, rigorous simulations also offer a means to estimate the losses originating from bulk scattering. In this work, a structure consisting of a transmitting transducer, two receiving split-finger transducers, a reflector placed between the receiving transducers, and gaps with different widths between the building blocks of the test structure (see Fig. 2), is used to address the scattering losses. The responses in the receiving transducers (ports 2 and 3), calculated in terms of the Y-parameters, contain contributions attributed to multiple reflections from the reflector and the transmitting (port 1) transducer. However, the reflections from the receiving

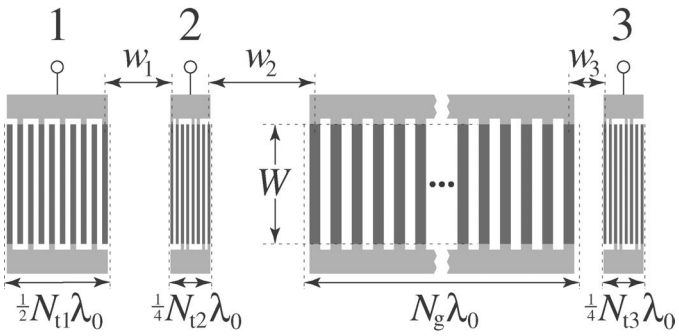

Fig. 2. Test structure for simulations of long reflectors. For 128° LiNbO$_3$, the values $N_{t1} = 10$, $N_{t2} = N_{t3} = 8$, $N_g = 80$, $\lambda_0 = 2$ μm, $W = 32$ μm, $w_1 = 100$ μm, $w_2 = 170$ μm, and $w_3 = 30$ μm are used.

transducers are negligible due to the split-finger geometry. Through time gating, the direct signal transmitted from the source transducer and received at the first split-finger transducer can be separated from the contribution of the signal reflected back from the grating. Correspondingly, the direct signal received in the second split-finger transducer can be identified.

The relatively small number of electrodes in the transducers implies that they are not optimized for SAW generation or reception. The reason for the split-finger geometry in the receiving transducers is an attempt to minimize the perturbation to the SAW caused by the IDT at port 2. Because of the mismatching, the minimal detectable level of SAW (see below) is limited by the spurious bulk waves and the EM feedthrough registered by the output transducers.

The bandwidth of an interdigital transducer, measured as the distance between the first zeros of the transfer function, can be estimated as

$$\mathrm{BW_{IDT}} = \frac{2}{N_{\text{finger pairs}}}. \tag{1}$$

Thus, choosing a small number of electrodes in the transmitting transducer (port 1) implies a wideband input signal. A large number of electrodes in the grating under investigation leads to a narrowband grating response, which can thus be analyzed accurately, see, e.g., Fig. 4.

The frequency step Δf and the simulation bandwidth B were chosen as 2 MHz and 1 GHz, thus, yielding a 501-point frequency grid. In the time domain, according to

$$\begin{aligned} T &= \frac{1}{\Delta f}, \\ \Delta t &= \frac{1}{\mathrm{B}}, \end{aligned} \tag{2}$$

the time span T and the interval between the temporal points Δt become 500 ns and 1 ns, respectively.

Using the rigorous FEM/BEM simulator, the duration of the calculation increases fast as a function of the overall number of electrode fingers. For example, with a 500-MHz PC, the simulation time for 501 frequency points for the test structure of Fig. 2 with 80 strips in the grating is about 13.5 h and that for 160 strips in the grating approaches 75 h.

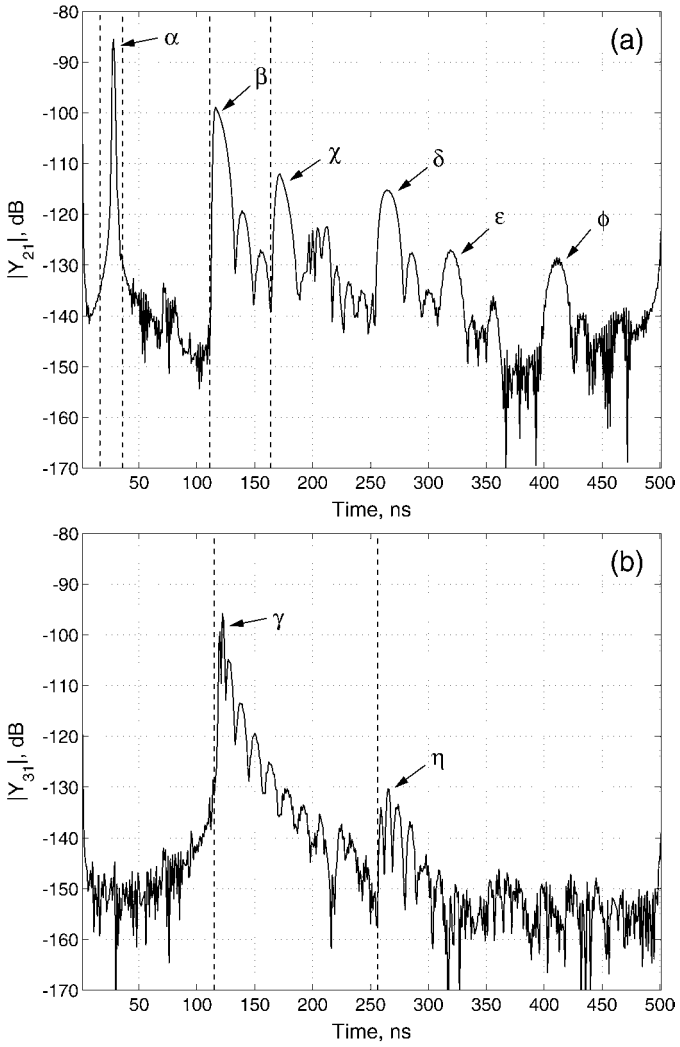

Fig. 3. Time-domain responses for the test structure in Fig. 2: (a) Signal transmitted from port 1 and received at port 2. (b) Signal transmitted from port 1 and received at port 3. The symbols refer to the different partial signals; see the text. The vertical dashed lines confine the contributions of the direct signal and the signal reflected once from the grating. Here, $a/p = 0.50$, $p = \lambda_0$, and $h/\lambda_0 = 5\%$.

IV. Time Gating

Inverse Fourier transform is used for the time gating. Typical illustrations of the signals observed at ports 2 and 3 are shown in the time domain in Fig. 3. In both of the figures, the vertical dashed lines denote the truncation limits used in the time-gating procedure.

In Fig. 3(a), the different signal contributions are labeled α–ϕ. Taking the SAW velocity to be 3980 m/s, it is easy to see that the label α corresponds to the partial signal propagating the distance 100 μm directly from port 1 to port 2, see the description of the test structure in Fig. 2. The case β, corresponding to a propagation distance of about $100 + 170 + 170$ μm $= 440$ μm, is the first reflected contribution from the grating. Similarly, the partial signal labeled χ implies one reflection from the grating and another from the transmitting transducer (port 1). The responses δ, ϵ, and ϕ correspond to multiple reflections from

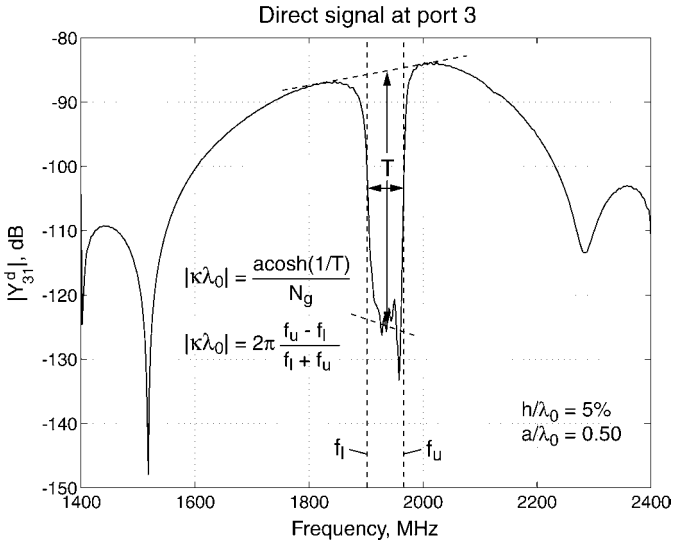

Fig. 4. Direct signal contribution transmitted from port 1 and received at port 3 in the frequency domain. The notch in the middle, a consequence of the grating stopband, is used to evaluate the reflectivity of the grating. Here, $a/p = 0.50$, $p = \lambda_0$, and $h/\lambda_0 = 5\%$.

the grating and port 1. Note that the response clearly indicates that the reflections from the split-finger transducer at port 2 can be neglected: the first contribution, including a reflection from port 2, is propagation three times across the gap w_1, i.e., 300 μm, which corresponds to a propagation time of about 75 ns.

Fig. 3(b) displays the signal transmitted from port 1 and observed at port 3. The first maximum, labeled γ, corresponds to the propagation distance of roughly $100 + 170 + 160 + 30$ μm $= 460$ μm, i.e., a direct propagation path through the grating. The peaks labeled η can be related to a triple-transit signal reflected once from the grating and once from the transmitting transducer.

The time-gated frequency response of the direct signal observed at port 3 ($|\mathrm{Y}_{31}^{\mathrm{d}}|$) is depicted in Fig. 4. The most apparent difference with respect to the direct signal received at port 2 ($|\mathrm{Y}_{21}^{\mathrm{d}}|$, see Fig. 7) is the notch originating from the grating stopband. In addition, losses occurring along the propagation path between ports 2 and 3 lower the power level of the signal.

The source being in port 1, it is justified to assume that the admittances observed at ports 2 and 3 are—via the electric currents at the ports 2 and 3, which they represent—proportional to the corresponding acoustic-wave amplitudes. Thus, energy comparison serves as a method for evaluating the losses

$$|\mathrm{Y}_{21}^{\mathrm{d}}|^2 \geq |\mathrm{Y}_{21}^{\mathrm{r}}|^2 + |\mathrm{Y}_{31}^{\mathrm{d}}|^2, \tag{3}$$

where the superscripts d and r refer to the direct and reflected signals, respectively.

In what follows, the results of the simulations are interpreted in the framework of the COM model.

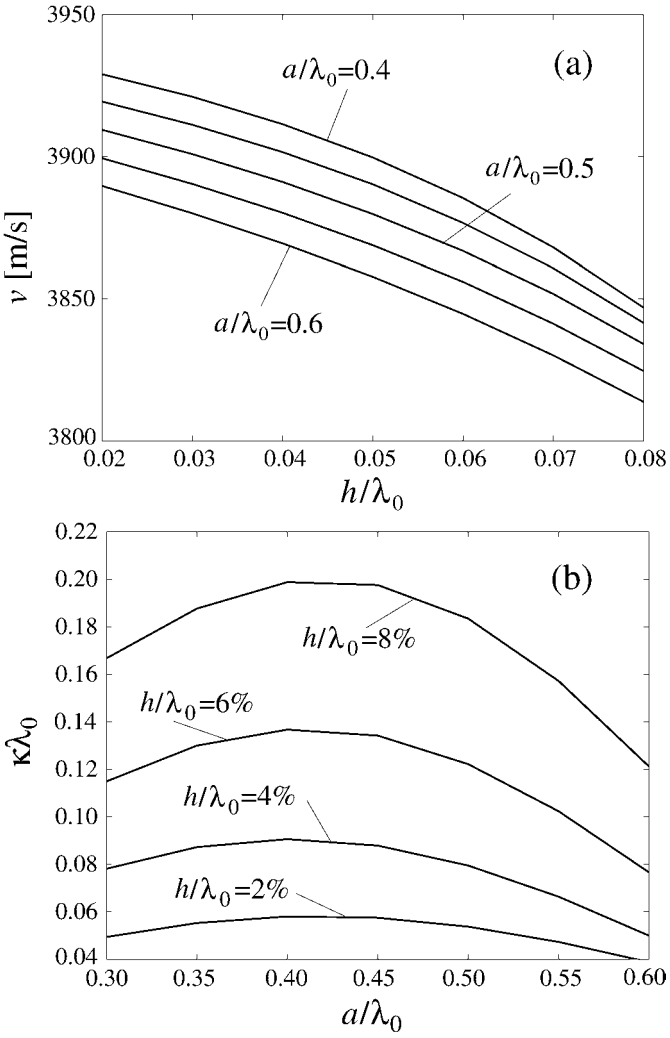

Fig. 5. (a) Velocities and (b) reflectivities for second-harmonic reflectors on 128° YX-cut $LiNbO_3$, determined from simulations of infinite periodic gratings.

V. Results of Simulations of Infinite Periodic Arrays

The periodic structure simulator with mechanical sources was used to determine the velocity and reflectivity on the 128° YX-cut $LiNbO_3$, supporting a Rayleigh wave, as functions of the metallization ratio, a/λ_0, and the relative electrode thickness, h/λ_0. The materials parameters by Kovacs *et al.* [10] were used for $LiNbO_3$. The aluminum electrodes were assumed rectangular and isotropic.

The velocities and reflectivities obtained are illustrated in Fig. 5. The velocities are notably (almost 50 m/s) higher than those for operation at the fundamental frequency. The effect is probably due to the reduced screening of the electric fields by the electrodes. The velocities tend to be quite sensitive to the metallization ratio. Consequently, even though the critical dimensions are twice as large as they would be if reflectors operating at the fundamental frequency were used instead, precise control over the electrode width may nevertheless be required.

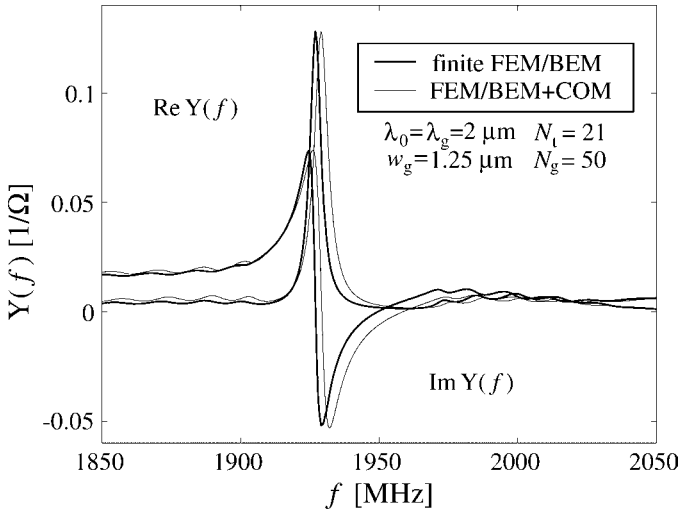

Fig. 6. Simulated resonator response vs. COM model on 128° YX-$LiNbO_3$ with $h/\lambda_0 = 5\%$ and metallization ratio 0.5. The structure is of the type shown in Fig. 1(a).

The reflectivity increases strongly with the electrode thickness, reaching a value as high as 20% for $h/\lambda_0 = 8\%$. Such an excellent reflectivity is a somewhat unexpected result, especially when compared with the rather poor reflectivity for the fundamental harmonic. For all the thicknesses studied, the maximum reflectivity is achieved for a/λ_0 close to 0.4.

VI. Results of Rigorous Simulations

In further studies, a rigorous FEM/BEM simulator [6] was utilized to obtain improved estimates for the reflectivity and the attenuation for Rayleigh waves in a long reflector on 128° YX-cut $LiNbO_3$. Again, the materials parameters by Kovacs *et al.* [10] were used, and the aluminum electrodes were assumed rectangular and isotropic.

The simulation of a finite one-port resonator with $h/\lambda_0 = 5\%$ and $a/p = 0.5$ is displayed in Fig. 6. Also shown is the admittance obtained from COM with the parameters determined from the periodic FEM/BEM simulations. The agreement is reasonable. No significant attenuation is predicted in the simulations, suggesting that the second-harmonic reflectors on 128°-cut $LiNbO_3$ indeed are promising for applications demanding high reflectivity.

A. Attenuation

The energy balance, derived from the simulation results for the test structure (see Fig. 2) having the particular grating geometry of $h/\lambda_0 = 5\% \mathrel{\hat{=}} 1000$ Å and $a/p = 0.5$, is shown in Fig. 7. The inequality in (3) is clearly manifested.

For reflectors operating at the second harmonic, it can be readily seen that in the reflector passband regions close to the stopband, the total losses are on the order of 5 to 7 dB. This value is about one order of magnitude higher than that estimated for the fundamental mode of operation, around 0.7 to 1.2 dB.

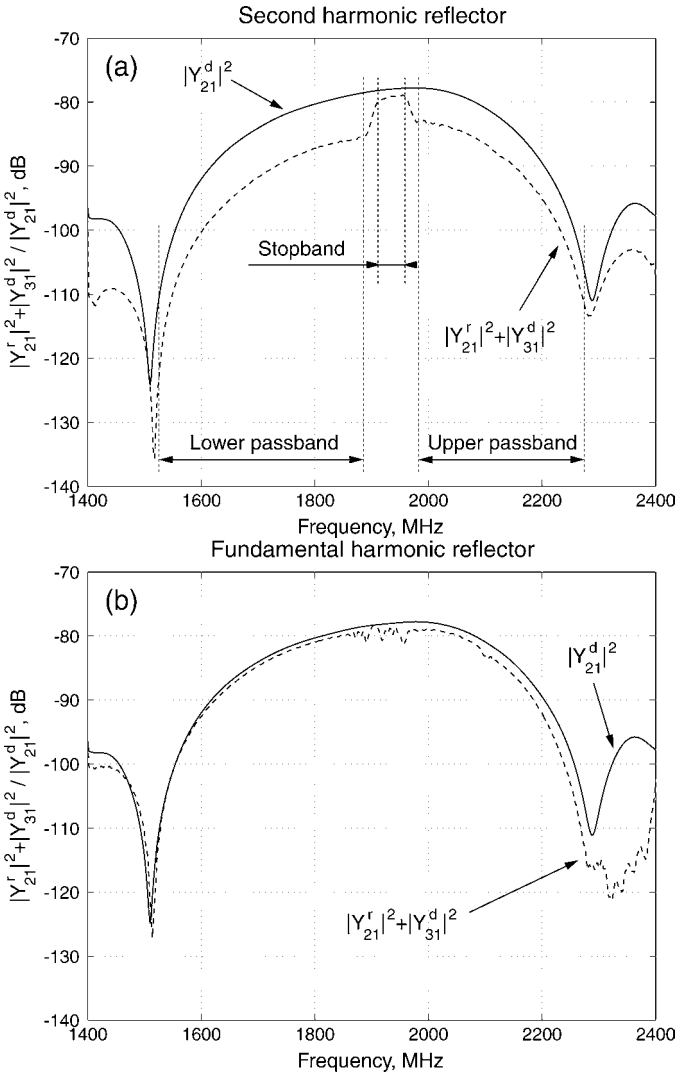

Fig. 7. (a) Energy balance for the structure shown in Fig. 2. The dashed vertical lines indicate the grating stopband and the lower and upper passbands. (b) The energy balance for an equivalent test structure with the reflector operating at the fundamental frequency ($N_g = 160$, $p = \lambda_0/2$). The substrate is 128° YX-$LiNbO_3$ with $h/\lambda_0 = 5\%$ and metallization ratio 0.5.

However, in the reflector stopband region, the attenuation is significantly reduced for the second-harmonic mode of operation (see dashed curve in Fig. 7(a)), while no systematic change is observed for the fundamental-mode reflector (see dashed curve in Fig. 7(b)). Actually, we see little, if any, increase in the losses in the stopband compared with the case of the fundamental harmonic reflector. This is likely to be the consequence of the short penetration depth of the wave into the reflector due to the high reflectivity. Hence, the losses attributed to scattering, present in the whole frequency range, are limited in the stopband. Furthermore, a comparison of simulations, including and excluding resistivity, suggests that the resistive losses are practically negligible in the second-harmonic reflector, while for the fundamental harmonic operation, it can not be justified to disregard the resistivity, at least for large apertures.

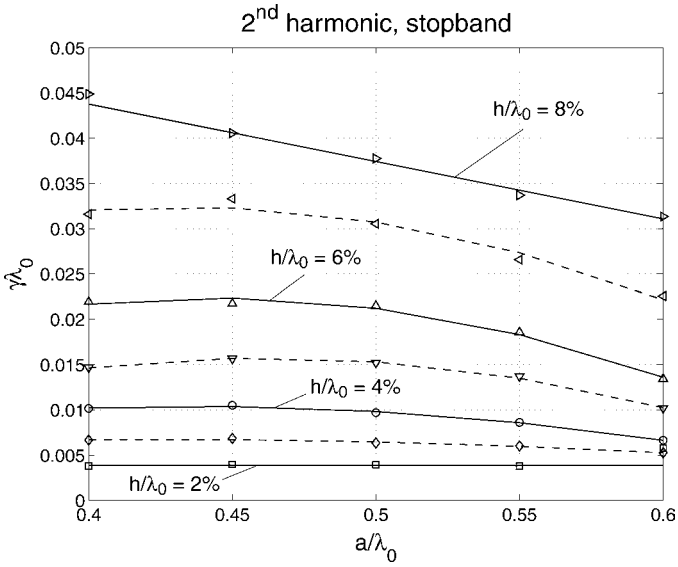

Fig. 8. Attenuation in the stopband normalized to the effective penetration depth in units of λ_0, $|\kappa\lambda_0|^{-1}$ for the grating operating at the second harmonic as a function of a/λ_0 and h/λ_0.

Fig. 8 shows the attenuation in the grating stopband for operation at the second harmonic frequency, obtained via rigorous simulations for the test structure of Fig. 2, as a function of a/λ_0 and h/λ_0. Attenuation values for the second-harmonic grating in the lower and upper passbands, taken as frequency ranges between the notches and the stopband in the energy balance image (see Fig. 7), are shown in Fig. 9. Only the total losses are calculated from the energy balance. To define the attenuation coefficient (per wavelength), we normalize these losses to the length of the grating. However, this procedure would not have much sense for stopband frequencies. In the grating stopband, as opposed to the total grating length in λ_0 in the passband, the losses are normalized to $|\kappa\lambda_0|^{-1}$, the effective penetration depth into the grating given by the COM model. The resulting attenuation in the stopband is roughly twice the value for the passband attenuation.

For the fundamental harmonic, the losses in the passband are smaller than those for the second-harmonic grating (see Fig. 7). In the stopband, the evaluation of losses is often aggravated due to ripples originating from the time-gating procedure. Therefore, the values obtained are subject to a larger uncertainty than those for a grating operating at the second harmonic. Most of the attenuation values obtained for the fundamental harmonic case, in Nepers, were between $\gamma\lambda_0\big|_{\mathrm{LPB}} = 0.8\ldots1.05\cdot10^{-3}$, $\gamma\lambda_0\big|_{\mathrm{SB}} = 0\ldots1.5\cdot10^{-3}$, and $\gamma\lambda_0\big|_{\mathrm{UPB}} = 2\ldots4\cdot10^{-3}$, in the lower passband, stopband, and the upper passband, respectively.

The origin of this attenuation, although not studied in detail, is in the intrinsic material losses included in the calculations of Green's functions within the FEM/BEM software, scattering at the ends of the grating, and resistive losses due to the finite conductivity.

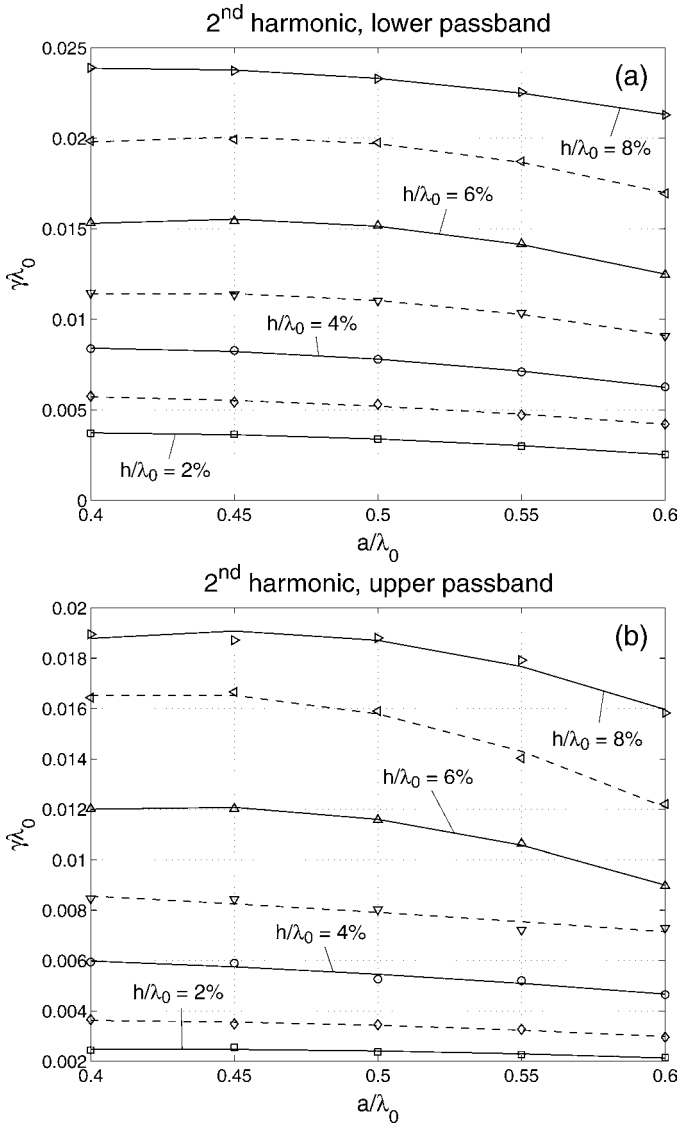

Fig. 9. Attenuation in the passband normalized to the length of the grating, in units of λ_0, operating at the second harmonic as a function of a/λ_0 and h/λ_0. (a) Lower passband. (b) Upper passband.

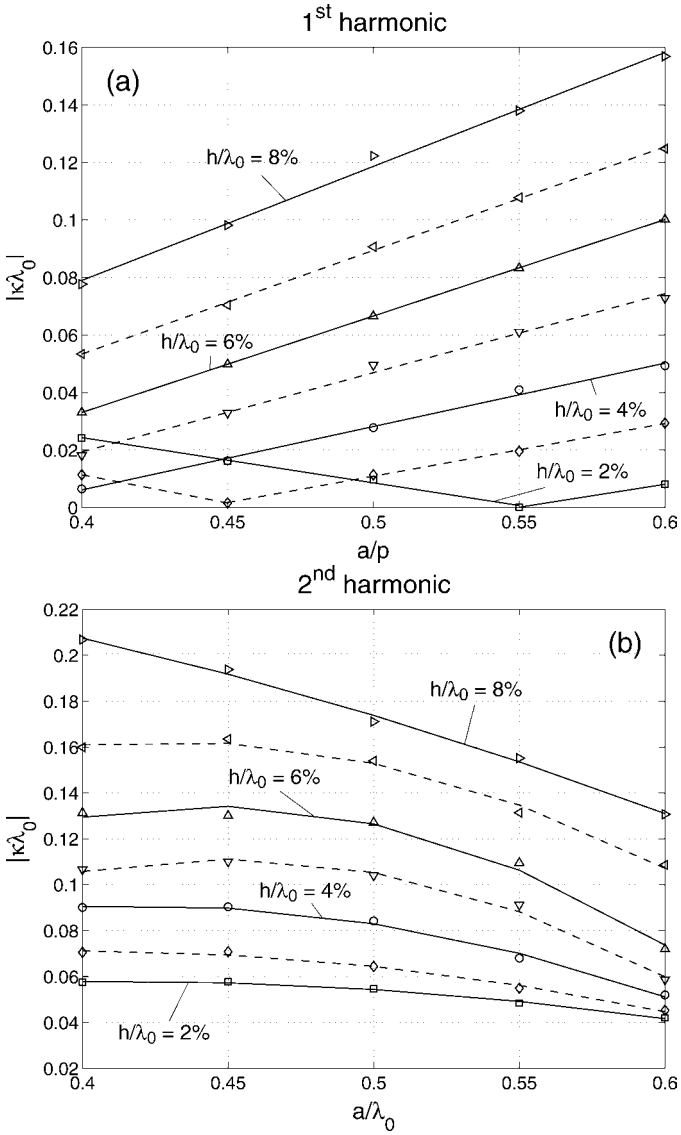

Fig. 10. Reflectivity as a function of a/p and h/λ_0. (a) Grating operating at the fundamental harmonic ($N_g = 160$, $\lambda_0 = 2p$). (b) Grating operating at the second harmonic ($N_g = 80$, $\lambda_0 = p$).

B. Reflectivity

The reflectivity per wavelength $|\kappa\lambda_0|$ can be estimated from Y_{31} (see Fig. 4) as

$$\mathrm{T} = \frac{1}{\cosh\left(|\kappa\lambda_0| N_{\lambda_0}\right)}, \tag{4}$$

where T is the amplitude transmission coefficient of the grating at the center of its stopband, and N_{λ_0} is the length of the grating in units of λ_0. The resulting value for the test structure with $N_g = 80$, $h/\lambda_0 = 5\%$, and $a/\lambda_0 = 0.5$ is found to be about 6.5%, less than the 10% calculated for an infinite periodic structure.

However, especially if the reflectivity is large, the depth of the notch in Fig. 4 is subject to a considerable uncertainty. This is due to the relatively low SAW amplitude level (see Section III), the stepsize of the frequency grid and the time-gating procedure. In order to obtain an improved approximation for $|\kappa\lambda_0|$, we use for the width of the stopband

$$\frac{|\kappa\lambda_0|}{\pi} = \frac{\mathrm{SBW}}{f_0} \Leftrightarrow |\kappa\lambda_0| = 2\pi\frac{f_\mathrm{u} - f_\mathrm{l}}{f_\mathrm{l} + f_\mathrm{u}}, \tag{5}$$

where f_l and f_u are the frequencies denoting the lower and upper edges of the stopband, respectively, and $\mathrm{SBW} = f_\mathrm{u} - f_\mathrm{l}$ stands for its width. Since the level at which the stopband is evaluated affects the result, we use an iteration procedure where the expression for the above theoretical amplitude transmission coefficient is used to evaluate the actual minimum level at the notch and, further, the correct level for stopband width. For low reflectivities, this method suffers from the large stepsize in the frequency grid, and (4) is utilized as such, instead.

The reflectivities obtained for gratings operating at the fundamental and second-harmonic frequency, expressed in $|\kappa\lambda_0|$, are shown in Fig. 10. The results are in good agreement with those obtained via FEM/BEM simulations for infinite periodic structures (see Fig. 5).

VII. Discussion

We have numerically investigated long reflectors operating at the second-harmonic frequency on 128° $LiNbO_3$. A FEM/BEM simulator for infinite periodic arrays and a rigorous FEM/BEM simulator were used. The results obtained suggest that high reflectivities can be achieved with reasonable electrode thicknesses.

According to our simulations, the losses due to BAW scattering inside the grating with periodicity $p = \lambda_0$ increase proportionally to the thickness of the aluminium electrodes. Outside the stopband, they are significantly higher than those for the fundamental-mode reflector with $p = \lambda_0/2$. However, inside the stopband we observe a strong decrease of the losses since the SAW penetrates only a limited distance inside the grating, and the waves are reflected before having the chance to dissipate their energy via scattering into the bulk of the substrate.

References

[1] R. C. M. Li and J. Melngailis, "The influence of stored energy at step discontinuities on the behaviour of surface-wave gratings," *IEEE Trans. Sonics Ultrason.*, vol. 22, pp. 189–198, May 1975.

[2] K.-Y. Hashimoto, *Surface Acoustic Wave Devices in Telecommunications*. Berlin: Springer, 2000, p. 27.

[3] S. V. Biryukov, Y. V. Gulyaev, V. V. Krylov, and V. P. Plessky, "Surface Acoustic Waves," in *Inhomogenous Media*. Berlin: Springer, 1995, pp. 320–321.

[4] C. K. Campbell and P. J. Edmonson, "Conductance measurements on a leaky SAW harmonic one-port resonator," *IEEE Trans. Ultrason., Ferroelect., Freq. Contr.*, vol. 47, pp. 111–116, Jan. 2000.

[5] J. Koskela, V. P. Plessky, and M. M. Salomaa, "SAW/LSAW COM parameter extraction from computer experiments with harmonic admittance of a periodic array of electrodes," *IEEE Trans. Ultrason., Ferroelect., Freq. Contr.*, vol. 46, pp. 806–816, July 1999.

[6] P. Ventura, J. M. Hodé, M. Solal, J. Desbois, and J. Ribbe, "Numerical methods for SAW propagation characterization," in *Proc. IEEE Ultrason. Symp.*, 1998, pp. 175–186.

[7] S. Lehtonen, J. Koskela, V. P. Plessky, and M. M. Salomaa, "Second harmonic reflectors," in *Proc. IEEE Ultrason. Symp.*, 2000, pp. 215–218.

[8] S. Lehtonen, V. P. Plessky, J. Koskela, and M. M. Salomaa, "Second harmonic reflectors on 128° $LiNbO_3$," in *Proc. IEEE Ultrason. Symp.*, 2001, pp. 139–143.

[9] P. Ventura, J. Desbois, and L. Boyer, "A mixed FEM/BEM analytical model of the electrode mechanical perturbation for SAW and PSAW propagation," in *Proc. IEEE Ultrason. Symp.*, 1993, pp. 205–208.

[10] G. Kovacs, M. Anhorn, H. E. Engan, G. Visintini, and C. C. W. Ruppel, "Improved material constants for $LiNbO_3$ and $LiTaO_3$," in *Proc. IEEE Ultrason. Symp.*, 1990, pp. 435–438.

Saku Lehtonen received the M.Sc. degree in technical physics from Helsinki University of Technology (HUT) in 1998. He is a postgraduate student in the Materials Physics Laboratory at HUT. His research interests include high-frequency SAW devices and characterization of SAW grating structures.

Victor P. Plessky (M'93–SM'01) received his Ph.D. degree in physical and mathematical sciences at the Moscow Physical-Technical Institute and the Dr.Sc. degree at the Institute of Radio Engineering and Electronics (IRE, Russian Academy of Sciences, Moscow) in 1978 and 1987, respectively. Beginning in 1978, he worked at IRE, first as a junior researcher, and, in 1987, he was promoted to the position of Laboratory Director. In 1991, he also worked as a part-time professor at the Patris Lumumba University, Moscow. He received the full professor title in 1995 from the Russian Government. In 1992, he joined ASCOM Microsystems SA in Bevaix, Switzerland, where he worked as a special SAW projects manager. Since 1997, he has lectured several courses on various SAW topics at Helsinki University of Technology as a visiting professor. Since 1998 he has been working at Thomson Microsonics (presently Thales Microsonics), from 2002 as a consultant. He has been engaged in research on semiconductor physics, SAW physics (new types of waves, scattering and reflection on surface irregularities, laser generation of SAW), SAW device development (filters, delay lines, RACs), and magnetostatic wave studies. Currently, his interests focus on SAW physics and low-loss SAW filter development. Professor Plessky is an IEEE Member. He was awarded the USSR National Award for Young Scientists in 1984.

Julius Koskela (M'98) received the M.Sc., LicTech, and DrTech degrees in technical physics from Helsinki University of Technology (HUT) in 1996, 1998, and 2001, respectively. His research interests include SAW physics and modeling SAW devices. After his doctoral dissertation, he joined the Nokia Group; he is currently working at Nokia Research Center. He is a member of the Finnish Physical Society.

Martti M. Salomaa (M'95) received his DrTech degree in technical physics from Helsinki University of Technology (HUT) in 1979. Thereafter, he worked at UCLA and the University of Virginia. From 1982 to 1991, he was the theory group leader at the Low Temperature Laboratory, HUT, and, from 1988 to 1991, he served as the director of the ROTA project between the Academy of Finland and the Soviet Academy of Sciences. He has held a sabbatical stipend at the University of Karlsruhe, and, in 1994, he was a guest professor at ETH-Zürich. Since 1996, he has been a professor of technical physics and the Director of the Materials Physics Laboratory in the Department of Engineering Physics and Mathematics at HUT. He is a corecipient of the 1987 Award for the Advancement of European Science (presented by the Körber Foundation, Hamburg). His research interests include BEC, superfluidity, superconductivity, magnetism, physics of SAW, nondiffracting waves, nanoelectronics, mesoscopic physics, and sonoluminescence. He is a member of the IEEE, APS, EPS, and the Finnish Physical and Optical Societies.